PHASE NOISE STUDIES AT THE ADVANCED PHOTON SOURCE*

N. S. Sereno[†], G. Decker, R. Lill and B. X. Yang, ANL, Argonne, IL 60439, USA

Abstract

Phase noise generated primarily by power line harmonics modulating the 352-MHz rf system in the APS storage ring is a dominant source of high-frequency beam motion, both longitudinally and transversely, due to dispersion in the lattice. It also places fundamental limits on the ability to generate picosecond-scale x-ray pulses for fast pump / probe experiments [1]. Measurements using turn-by-turn beam position monitors (BPMs) located at high-dispersion locations are compared and contrasted with results from a dedicated S-band phase detector connected to either a capacitive pickup electrode or a diamond x-ray detector. Horizontal beam position at high-dispersion locations is related directly to beam phase by a very simple relation involving the momentum compaction. Simulation results are used to validate this relationship and to quantify the relation between phase noise on the main rf vs beam arrival time jitter.

TRANSVERSE BEAM MOTION FROM LONGITUDINAL FLUCTUATIONS

Implicit in the BPM data analysis is that a position measurement can yield information about the longitudinal motion of the beam centroid through the dispersion at the BPM position. If the position measurement at the BPMs contains motion due to sources other than rf (amplitude and phase) noise (such as corrector, quad, dipole noise) determination of the phase noise by this approach is ambiguous compared to a direct phase measurement using a phase detector. From Eq. 8.18 of Wiedeman's text [2],

$$\frac{\partial \psi_n(t)}{\partial t} = -\beta c k_{\mathrm{h}}(\gamma^{-2} - \alpha)\frac{\Delta p_n(t)}{p_o}, \qquad (1)$$

which states that in the time domain, the rate of (rf) phase change of a particle in the bunch (denoted by n) relative to the synchronous particle is proportional to its momentum deviation from the synchronous particle. For our analysis, we simply want to measure the phase noise on the beam and don't ultimately care that this noise comes from rf system amplitude and phase fluctuations [3, 4]. For this purpose, Eq. 1 is sufficient for our analysis within certain limits.

For the case of the 7-GeV APS storage ring, $\beta \approx 1$, $\gamma^{-2} \approx 0$, the rf wavenumber $k_{\mathrm{h}} = \frac{\omega_{rf}}{c}$ and the ring lattice momentum compaction factor $\alpha = 2.83 \times 10^{-4}$. For a BPM where there is dispersion, Eq. 1 can be written in terms of the position offset since $x_n(t) = \eta \frac{\Delta p_n(t)}{p_o}$ where $x_n(t)$ is the position offset at the BPM, and η is the dispersion at the BPM. Expressed in terms of the centroid phase

and position measured by the BPM on each turn, Eq. 1 becomes,

$$\frac{\partial \psi(t)}{\partial t} = \frac{\alpha \omega_{rf}}{\eta} x(t). \qquad (2)$$

It is more convenient to write Eq. 2 in terms of the beam centroid arrival time (relative to the synchronous particle arrival time) at the cavity instead of phase using the constant rf frequency $\tau(t) = \psi(t)/\omega_{rf}$ resulting in,

$$\frac{\partial \tau(t)}{\partial t} = \frac{\alpha}{\eta} x(t). \qquad (3)$$

Note that if one substitutes the centroid momentum offset $\Delta p(t)/p_o = x/\eta$ into Eq. 3 the resulting equation looks similar to the definition of the first-order momentum compaction for a single particle. The two expressions do, however, differ by the time derivative on the left-hand side of Eq. 3.

We now turn to the frequency domain to express the centroid arrival time in terms of the BPM position offset. The frequency domain will also most clearly give us the domain of validity of Eq. 3. Taking the Fourier transform of both sides of Eq. 3 yields,

$$i\omega\tau(\omega) = \frac{\alpha}{\eta} x(\omega), \qquad (4)$$

where one sees an additional $1/\omega$ frequency dependence of the centroid time on position offset. The imaginary factor i indicates energy/position and (rf) time/centroid time motion differ by 90 degrees in phase. Since the PSD in each frequency bin for centroid time and position is proportional to the FFT amplitude of these quantities squared, using Eq. 4 one can write

$$\tau_{\mathrm{PSD}}(\omega) = \left(\frac{\alpha^2}{\eta^2 \omega^2}\right) x_{\mathrm{PSD}}(\omega), \qquad (5)$$

where we can obtain $x_{\mathrm{PSD}}(t)$ easily from the time domain FPGA BPM data using sddsfft [5]. For the APS storage ring, $\eta = 0.20$ m at the P5 BPMs and $\omega_{rf} = 2\pi f_{rf}$ and $f_{rf} = 351.9355$ MHz. The mean square beam centroid time motion is then easily obtained from Eq. 5 by integration (or reverse integration) over the frequency band of interest.

We undertook a simulation study using bf elegant [6] to validate Eqs. 3 and 5. We used 1000 particles and tracked them using linear tracking for 1 second to directly compare to the FPGA BPM and phase detector measurements. The tracking produced motion over a frequency band 1 Hz to 135 kHz (Nyquist limit) for various sources of impressed rf system noise. Elegant tracking output included the temporal centroid and B:P5 horizontal centroid values on each turn. We then used the centroid output to directly verify

both left and right sides of Eqs. 3 and 5. We thereby demonstrated the validity of the analytic calculation in both time and frequency domains via simulation.

In the frequency domain, it is known that below about 200 Hz, beam motion at the BPMs becomes dominated by magnet sources compared to the rf system since the shielding effect of the vacuum chamber becomes less at low frequency. The fast correctors used in the real-time feedback system have bandwidth going up to 800 Hz due to their thinner chamber. The metal-coated ceramic kicker chambers also would admit fields at frequencies well beyond 200 Hz. However, during both the FPGA BPM and phase detector measurements the real-time feedback system (which drives the fast correctors at up to 1.5 kHz) was turned off as well as the kickers. So, we consider Eq. 5 valid for determination of phase noise above 200 Hz for the BPM data we analyzed.
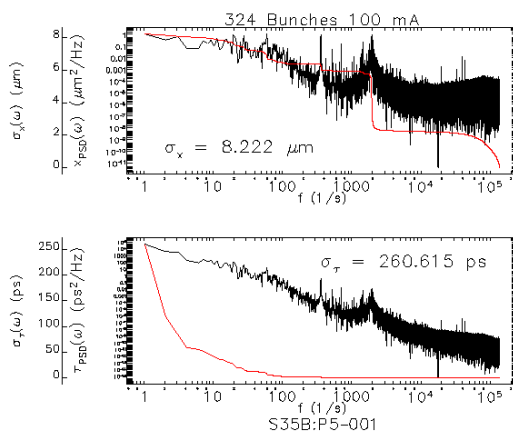
FPGA BPM DATA ANALYSIS

Figure 1: Sector 35 B:P5 FPGA BPM frequency domain data for 100 mA and 324 bunches. The top plot shows position data calculated using sddsfft, and the bottom plot shows frequency domain phase data derived using Eq. 5.
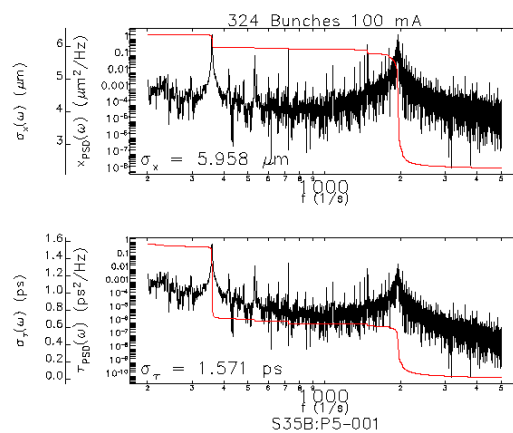

Figure 2: Sector 35 B:P5 BPM data at 100 mA and 324 bunches for data over the band 200 Hz to 5 kHz for comparison to Figure 1.

For the FPGA BPM experiment we took data using twelve high-dispersion "B:P5" FPGA BPMs at 100 and 150 mA for the storage ring most-used 24 bunch mode in addition to the 324 bunch mode. All feedback systems and pulsed magnets were turned off. The FPGA BPMs have the advantage of taking turn-by-turn data for up to 1 second in duration or 262144 turns. These BPMs were configured to average the position over all bunches in the fill pattern. Data analysis is performed using a script that calculates $\tau_{PSD}(\omega)$ using Eq. 5 and the calculated $x_{PSD}(\omega)$ from the FPGA BPM time domain data using sddsfft. The script then (reverse) integrates $\tau_{PSD}(\omega)$ over a user specified band of frequencies above 200 Hz and computes the rms phase noise in that band in ps. Note that due to the important factor of ω^{-2} in Eq. 5, $\tau_{PSD}(\omega)$ does not have the same frequency dependence as $x_{PSD}(\omega)$.

As an example of the data and processing, Figure 1 shows frequency domain position and (derived) phase data at 100 mA from data for the S35B:P5 BPM over the full band from 1 Hz to the Nyquist frequency 135.8 kHz. The top plot shows shows the PSD of the BPM position data and the reverse integrated rms position from sddsfft. The bottom plot shows the PSD phase and reverse-integrated rms phase derived from Eq. 5. Indicated on the plots is the total rms phase noise in ps and total rms position motion in the full band from 1 Hz to 135.8 kHz (8.2 μm position noise and 260.6 ps phase noise). One notices on the plots prominent features like the synchrotron tune at 2 kHz and a large line at 360 Hz due to the klystron rf systems. The most notable feature on the plot is the large increase in noise below about 200 Hz down to DC. As previously mentioned, this is due to the fact that below about 200 Hz, noise sources due to magnets start to dominate the motion. In addition, since the PSD phase shown on the bottom plot in Figure 1 is derived using Eq. 5, any noise source other than phase becomes enhanced due to the ω^{-2} factor in Eq. 5. We can see that use of the FPGA BPM data for phase noise measurements will be limited to frequencies above 200 Hz. We also limit the high-frequency point to 5 kHz so as to include the synchrotron tune. Beyond 5 kHz, the PSD phase noise becomes smaller like ω^{-2}, and hence frequencies above this point do not contribute significantly to the total integrated rms phase.

Figure 2 shows S35B:P5 data for 100 mA over the band 200 Hz to 5 kHz. The figures show essentially no rms phase motion due to frequencies beyond 5 kHz (bottom plot in the figure). This is partly due to the fact that the PSD for the phase motion is falling off at a rate given by ω^{-2}. One also sees that the rms position motion for frequencies above 5 kHz is about 2 μm. Both position and phase PSD curves show prominent synchrotron ($\approx$ 2 kHz) and 360-Hz features as seen in Figure 1. The 360-Hz line is known to come from the main rf systems and is presently being investigated by a dedicated mitigation effort. Comparing Figures 1 and 2, one sees the interesting result that the fraction of the rms position noise is 72% of the total rms motion over the complete bandwidth from 1 Hz to 135.8 kHz. Ta-

06 Instrumentation, Controls, Feedback and Operational Aspects

T24 Timing and Synchronization

ble 1 summarizes the FPGA BPM measurements for various beam currents, bunch patterns, and frequency bands of interest. One can see how much the line at 360 Hz from the main rf systems contributes to the total noise from 200 Hz to 136 kHz.

Table 1: Summary of FPGA B:P5 BPM phase noise measurements for various beam currents, bunch patterns and frequency bands.

Current (mA) / Bunch Pattern	Frequency Band	Phase Noise (ps)
100 - 150 / 24	340 - 380 Hz	0.4 - 1.5
	1 - 3 kHz	0.5
	200 Hz - 136 kHz	1.2 - 1.8
100 - 150 / 324	350 - 370 Hz	0.6 - 1.2
	200 Hz - 5 kHz	1.0 - 1.5

S-BAND PHASE DETECTOR MEASUREMENTS

An S-band phase detector (also called a beam arrival time (BAT) detector) has been implemented in sector 35 of the storage ring based on phase detector technology already in use for many years in the linac [7]. The beam induces a signal on the button electrode and is filtered using a band-pass filter tuned to a center frequency of 2.815 GHz with a 3-dB bandwidth of 3 MHz. The signal is then amplified and sent to the phase detector circuit. The detector's phase reference is derived from the SR rf master oscillator reference at 352 MHz multiplied to 2815 MHz. The calibration factor for the detector is 24 mV/ps. The phase detector output is therefore a measurement of the phase or beam arrival time relative to the rf master oscillator. Detection at 2815 MHz allows much better resolution of small phase errors on the order of a ps compared to detection at 352 MHz.
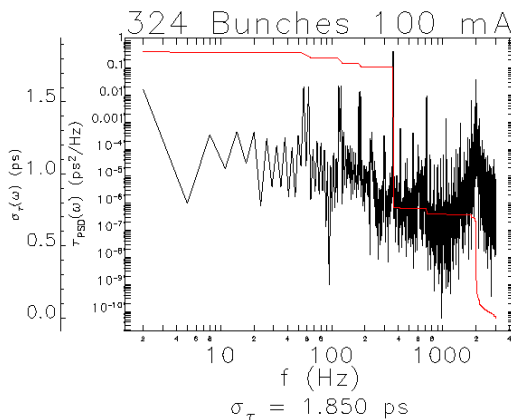

Figure 3: Phase detector frequency domain data taken for 324 bunches and 100 mA over the full band 2 Hz to 3 kHz.

Figure 3 shows phase detector data for 324 bunches and 100 mA taken at roughly the same time as the FPGA BPM data shown in Figures 1 and 2. The data in Figure 3 were taken over the band 2 Hz to 3 kHz with resolution bandwidth (RBW) of 3 Hz. Comparing Figures 1 and 3 one can see in the PSD phase spectrum the same synchrotron and 360 Hz lines. It turns out that the total integrated rms phase noise over the band in Figure 3 is almost the same as total integrated rms phase over the band 200 Hz to 5 kHz shown for the S35B:P5 BPM data in Figure 2. Table 2 summarizes the phase detector experiments. In general, the results agree closely with the data for the FPGA BPM phase noise measurements in the previous section. The table also shows results of a diamond detector exposed to the photon beam from sector 35 ID. For this experiment, the diamond detector was used in place of a BPM button. The outlier point of 17 ps for the 324 bunch case is likely an outlier due to a sudden shift in the main rf system phase.

Table 2: Summary of S-band phase detector phase noise measurements for various beam currents, bunch patterns and frequency bands including results using a diamond detector.

Current (mA) / Bunch Pattern	Frequency Band	Phase Noise (ps)
100 - 150 / 24	340 - 380 Hz	0.7 - 1.4
	1 - 3 kHz	0.5
	200 Hz - 136 kHz	1.0 - 1.6
100 - 150 / 324	2 Hz - 3 kHz	1.9 - 17
	200 Hz - 3 kHz	0.9 - 1.7
150 / 324 (Diamond)	3 Hz - 4 kHz	1.8
	200 Hz - 4 kHz	1.6

REFERENCES

[1] A. Zholents et al., NIM A 425, 385 (1999).

[2] H. Wiedemann, *Particle Accelerator Physics: Basic Principles and Linear Beam Dynamics*, (Springer-Verlag, 1993), 272.

[3] J. M. Byrd, "Effects of Phase Noise in Heavily Beam Loaded Storage Rings," Proceedings of the 1997 PAC, pp. 1806-1808, (1999); http://www.JACoW.org

[4] K. W. Ormond and J. T. Rogers, "Synchrotron Oscillation Driven by RF Phase Noise," Proceedings of the 1997 PAC, pp. 1822-1824 (1997); http://www.JACoW.org

[5] M. Borland, "M. Borland, "A Self-Describing File Protocol for Simulation Integration and Shared Postprocessors," 1995 PAC, Dallas, Texas, 2184 (1996); http://www.JACoW.org

[6] M. Borland, "elegant: A Flexible SDDS-Compliant Code for Accelerator Simulation," Advanced Photon Source Light Source Note ANL/APS/LS-287, September 2000.

[7] N. S. Sereno et al. Phys. Rev. ST Accel. Beams 11, 072801 (2008).